Development of a U-19Pu-10Zr Fuel Performance Benchmark Case Based on the IFR-1 Experiment

Ian Greenquist*[a], Kaylee M. Cunningham[b], Jianwei Hu[a], Jeffrey J. Powers[a], Douglas C. Crawford[c]

a: Nuclear Energy and Fuel Cycle Division, Oak Ridge National Laboratory, Oak Ridge, Tennessee
b: Department of Materials Science and Engineering, University of Florida, Gainesville, Florida
c: Materials and Fuels Complex, Idaho National Laboratory, Idaho Falls, Idaho
**Corresponding author: greenquistit@ornl.gov*

ABSTRACT

Metallic nuclear fuels are subject to research and development for use in advanced reactors. Robust, accurate metallic fuel performance models are important for the design, safety analysis, and licensing of these reactors. However, metallic fuel performance models require additional development; they are not as mature as UO_2 fuel performance models. A benchmark case based on the IFR-1 experiment was developed to better gauge the accuracy of existing models, identify models for high-priority development, and potentially quantify any future improvements made by further model development.

This work collected publicly available information on the IFR-1 experiment and used it to develop the benchmark case. Fuel behavior during the IFR-1 irradiation was simulated by using the fuel performance code BISON, and the predicted results were compared with postirradiation examination data from the IFR-1 experiment. A sensitivity study and tuning studies were performed as a preliminary investigation into the causes of inaccurate temperature and dimensional change predictions.

The benchmark predicted reasonably accurate values for the burnup and fission gas release. There was error in the predicted temperatures, which could be explained by uncertainty in the input parameters and legacy temperatures. BISON over-predicted dimensional changes in the fuel and cladding. The sensitivity study showed that the dimensional changes were most sensitive to the fuel swelling anisotropy and the cladding void swelling model. Future benchmark and model development should focus on cladding swelling behaviors to improve dimensional change predictions.

KEYWORDS: U-Pu-Zr, fuel performance, BISON, sensitivity analysis

1. INTRODUCTION

UO_2 is the dominant nuclear fuel worldwide and is well-established for use in light water reactors, Canada Deuterium Uranium (CANDU) reactors, and Advanced Gas Reactors. Decades of research and development have gone into fuel performance models for this ceramic fuel type. Far less development has been devoted to U-Zr-based metallic fuel performance models [1, 2, 3, 4, 5]. Currently, the US

Department of Energy (DOE) is considering the use of metallic fuel (either U-Zr or U-Pu-Zr) for a possible new test reactor [6, 7], and several private companies are considering metallic fuels in novel reactor designs [8, 9]. Because of these developments, a new focus has been placed on developing accurate fuel performance models to support reactor design, experiment design, and safety qualification for metallic fuels.

One way to gauge the accuracy of existing and future metallic fuel performance models is through the use of benchmark cases. Benchmark cases are fuel performance simulations of irradiation experiments that compare the predicted results with the corresponding legacy results. Benchmark cases aid in the development of fuel performance models in several ways. First, they enable the assessments of the accuracy of existing models. Second, any inaccurate predictions can be used to identify models for high-priority development. Third, they can be used to quantify the subsequent improvements made by new or updated models.

This work details the development of a benchmark case for 71 wt. % U, 19 wt. % Pu, 10 wt. % Zr (U-19Pu-10Zr) metallic fuel based on the IFR-1 experiment. The IFR-1 experiment was one of seven full-size fuel assemblies irradiated during the Integral Fast Reactor (IFR) program and was the only full-size assembly to include U-Pu-Zr fuel rods [10].

The IFR concept was developed by Argonne National Laboratory during the late 1980s and early 1990s [11], and its technology underlies the US Advanced Liquid Metal Reactor program [12] and GE Hitachi's PRISM (Power Reactor Innovative Small Module) reactor [13].The goal of the program was to update and commercialize the technology used in Experimental Breeder Reactor II (EBR-II), a Na pool-type fast reactor [13]. Most experiments for the IFR were irradiated in EBR-II, but a full-size IFR fuel pin could not be irradiated in EBR-II because the IFR design called for longer fuel pins [10]. Thus, the IFR-1 experiment was irradiated in the Fast Flux Test Facility (FFTF) in Hanford, Washington to identify any long-rod effects not observed in EBR-II fuel rods [14].

The FFTF was a loop-type Na-cooled fast-spectrum test reactor that operated between 1982 and 1992. It had a larger test volume than EBR-II and transient testing capabilities [15]. The IFR-1 experiment was irradiated between September 1986 and October 1988 to a target peak burnup of 10 at. %. Researchers were interested in comparing the neutronic and mechanical effects of full-length IFR pins with those seen in EBR-II's shorter test pins.

The experiment, including irradiation conditions and postirradiation examination (PIE) results, was documented in three sources: a 1992 conference paper [16], a 2011 Idaho National Laboratory (INL) report [10], and a 2012 peer-reviewed journal article based on the 2011 report [17]. There are some inconsistencies in the data reported in the three sources such as the shape of the axial heat generation distribution. In these cases, one of the original authors of the three sources determined that the 2011 report was generally the most complete and reliable [18]. This work includes a comprehensive description of the IFR-1 benchmark case and its implementation in BISON. BISON predictions were compared to legacy measurements [10]and calculations, including burnup, temperatures, fuel and cladding strains, and fission gas release (FGR) fractions. While there are other important values that BISON can predict—such as stresses—these predictions are not included in this work because no corresponding legacy values could be found to gauge the accuracy. Preliminary studies to identify BISON models that could be contributing to inaccurate predictions were also performed. Finally, recommendations are made for further benchmark development and potential areas for additional BISON development.

BISON is a fuel performance code maintained by INL and under active development at a variety of laboratories and universities. As such, the BISON predictions presented in this work are likely to change over time and have changed since previous versions of the benchmark results were last reported [19]. The work presented here is not meant to validate nor criticize current or future BISON versions. It is meant as a snapshot of current BISON accuracy and to aid in the future development of the code. All simulations for this work used a BISON version from June 24, 2020[*].

2. SUMMARY OF SELECT BISON MODELS

A complete description of BISON models and capabilities is beyond the scope of this work but can be found in the BISON documentation [20, 21]. Only governing equations of the models of interest in this benchmark case are summarized here. The primary equations governing BISON simulations are conservation of energy, conservation of mass, and conservation of momentum [21]. Conservation of energy is described by the heat transport equation,

$$\rho C_p \frac{\partial T}{\partial t} - \nabla \cdot (k \nabla \mathrm{T}) - e_f \dot{F} = 0, \tag{1}$$

where ρ is the density, C_p is the specific heat, T is the temperature, k is the thermal conductivity, e_f is the average energy produced per fission, and $\dot{F}$ is the fission rate. The conservation equation for a given species is

$$\frac{\partial C}{\partial t} - \nabla \cdot (D \nabla C) + \lambda C - S = 0, \tag{2}$$

where C is the concentration, D is the diffusion coefficient, λ is the radioactive decay constant, and S is a source term. Conservation of momentum is described by Cauchy's equation,

$$\nabla \cdot \boldsymbol{\sigma} + \rho \boldsymbol{f} = \mathbf{0} \tag{3}$$

where $\boldsymbol{\sigma}$ is the Cauchy stress tensor and $\boldsymbol{f}$ is the body force per unit mass (such as gravity). The primary solution variable is displacement, which is connected to the stress field via strain through a constitutive relationship.

Local burnup, $\beta(\vec{x})$, is an important calculated variable correlated to other models such as swelling and fission gas release. It is based on the local fission rate, $\dot{F}(\vec{x}, t)$, and the initial fuel atom density $N_f^0(\vec{x})$,

$$\beta(\vec{x}) = \int \frac{\dot{F}(\vec{x}, t)}{N_f^0(\vec{x})} dt, \tag{4}$$

where $\vec{x}$ is the position vector.

Equations (1)–(4) are all analytical models. They are derived from relevant physics theories and have been successfully applied to multiple systems. However, some of the fast-reactor-specific correlations that go into these equations are empirical relationships. For example, the thermal conductivity of U-Zr-based fuels is based on fitting an equation to experimental data. Due to a lack of experimental data with

[*] git commit `45096d10ec4faeb6e1bba1a1ac99e553f3a18a2a`

irradiated fuels, the irradiation effects on these equations are often the most uncertain models in BISON U-Zr predictions.

Also of interest for this work are the fission gas production and release models for metallic fuels. The amount of fission gas produced is described by the function,

$$G_p(\vec{x},t) = \int \frac{\dot{F}(\vec{x},t)\gamma}{N_A} dt, \tag{5}$$

where G_p is the amount of fission gas produced in moles, γ is the yield of gas atoms per fission, and N_A is Avogadro's number. The amount of fission gas released, $G_r(\vec{x},p,t)$, is calculated as

$$G_r(\vec{x},p,t) = \begin{cases} 0, & p < p_c \\ \alpha_0 G_p(\vec{x},t), & p = p_c \\ \alpha_0 G_p(\vec{x},t_c) + \alpha_c \int_{t_c}^{t} G_p(\vec{x},t')dt', & p > p_c \end{cases}, \tag{6}$$

where p and p_c are the porosity (as determined by the fission gas swelling model) and a critical porosity, respectively, α_0 and α_c are the initial FGR fraction and post-critical FGR fraction, respectively, and t_c is the time at which critical porosity was reached. Equation (5) is an analytical equation, while Equation (6) is a semi-empirical equation. The form of Equation (6) is based on physics theory, but the individual terms such as p_c, α_0, and α_c can only be determined by fitting the model to match experimental data.

These equations govern the predictions of interest in the current work but are not comprehensive and do not capture feedback and nonlinear effects. For example, fission gas production causes pore growth, which increases the stress of the system, directly affecting the displacements and dimensional changes. Pores also degrade thermal conductivity, which in turn causes the temperature in the fuel to increase. That causes additional displacements through thermal expansion and thermal creep. So, Equation (5) affects Equation (3) both directly and indirectly. For more complete descriptions of feedbacks and nonlinear effects, see the BISON documentation [20, 21].

3. IFR-1 BENCHMARK CASE

Because of the low availability of pin-specific measurements and calculations, this benchmark case was set up as a representative generic U-19Pu-10Zr pin rather than any specific pin. For each of the time-dependent predicted results considered, all available legacy measurements and calculations were included for comparison.

3.1. PROBLEM GEOMETRY

The IFR-1 test assembly consisted of 169 fuel pins in a hexagonal assembly. Of the pins, 18 contained U-19Pu-10Zr alloy fuel, 19 contained U-8Pu-10Zr alloy fuel, and the remainder contained U-10Zr alloy fuel. The U enrichment was adjusted for each alloy to maintain the same approximate heat generation rate. All the pins were clad in 20% cold-worked D9 stainless steel [22] and were wrapped in 1.37 mm diameter D9 wire that served as a spacer between pins and as a turbulence generator to improve mixing and thermal transport of the Na coolant. However, the wires were not included as part of the simulation mesh.

The active fuel column of each pin was made of three slugs with a combined length of 914 mm. These slugs were sandwiched between two 165 mm blanket slugs typical of use in an axial blanket. The blankets were composed of a U-10Zr alloy with depleted U. The radial gap between the slugs and the cladding was filled with Na.

The cladding had an external diameter of 6.86 mm and a wall thickness of 0.56 mm. The total cladding length was 2,377.4 mm. The 2011 report [10] stated that at operating temperatures, the fuel/plenum ratio was 1.0. However, the amount of Na was not recorded, so the exact length of the plenum could not be determined. Additionally, no measurements are given for the cladding ends. The top of the cladding had a solid machined section meant for handling the fuel in a hot cell [10]. The bottom end plug configuration included provisions to hold it in place inside the assembly [2, 10].

The dimensions used in the benchmark case are shown in Figure 1. The end caps were modeled as flat with a thickness of 3 mm. This approximation does not match the actual end caps but significantly simplifies the mesh. During benchmark development, several thicknesses were tested, and the end cap thicknesses was determined to not significantly impact the predicted results [19]. A small gap of 0.4 mm was also included between the bottom end cap and the bottom blanket slug to prevent computationally expensive contact between the bottom blanket at the cladding. This gap is not necessarily physically accurate, but the approach improves the computational stability and efficiency with negligible impact on the benchmark accuracy.

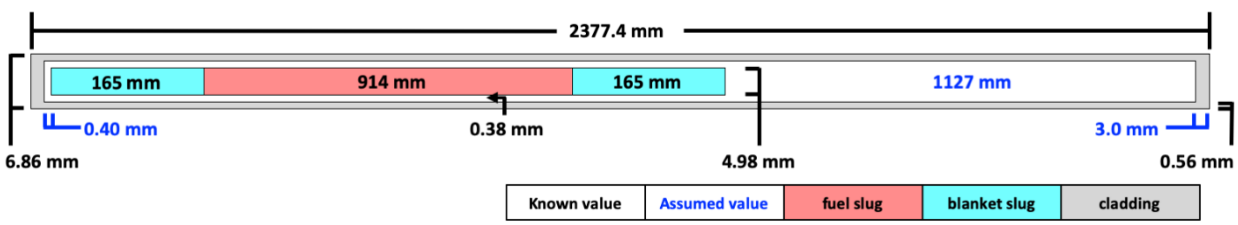

Figure 1. Benchmark case cross-sectional dimensions (not to scale). Black text indicates values from the IFR-1 report [10]*, and blue text indicates values that had to be assumed.*

For the BISON simulation, a 2D-RZ axisymmetric mesh was used rather than a full 3D mesh. This was much more computationally efficient and was not expected to impact the predictions because no azimuthal variations were known or modeled. The fuel slug mesh was glued to the blanket meshes, eliminating the need to model contact at the fuel-blanket interfaces.

3.2. LINEAR HEAT GENERATION RATE

The linear heat generation rate (LHGR) is a primary input into fuel performance simulations. It specifies the energy output of the fuel pin as a function of time and axial position within the fuel. As is commonly done in BISON, the LHGR was treated as a product of two functions: the time dependent average LHGR, $\overline{LHGR}(t)$, and the spatially dependent peaking factor, $p(z)$:

$$LHGR(t,z) = \overline{LHGR}(t)p(z), \tag{7}$$

where t is the time, and z is the axial position in units of length. Because the peaking factor was meant to reflect deviation from the average, it had the additional constraint:

$$\frac{1}{z_t - z_b} \int_{z_b}^{z_t} p(z)dz = 1, \tag{8}$$

where z_b and z_t represent the axial positions of the bottom and top of the active fuel column, respectively.

The IFR-1 experiment ran over the course of six FFTF operating cycles: 9A, 9B, 9C, 10A-1, 10A-2, and 10B. The INL report included equivalent full-power days (EFPDs) for each operating cycle, as well as the assembly average LHGR for nearly every beginning of cycle (BOC) and end of cycle (EOC). The only exception was that no LHGR was recorded for cycle 10A-1 EOC. For convenience, it was assumed that the 10A-1 EOC LHGR matched the 10A-1 BOC LHGR.

The power history used in the benchmark case is shown in Figure 2. It began with a coolant inlet temperature of 298 K and an average LHGR of 0 kW m^{-1}. Over 1 hr, the coolant inlet temperature increased to 633 K [10], and the average LHGR increased to cycle 9A's BOC average LHGR of 39.6 kW m^{-1}. The cycle 9A simulation lasted for 138 days to match the legacy EFPD, during which time the average LHGR was modeled to decrease linearly to the 9A EOC average LHGR of 36.5 kW m^{-1}. After 9A EOC, 1 hr was added to simulate the transition to 9B BOC average LHGR. The simulation followed this pattern for the remaining cycles with a constant coolant inlet temperature. Shutdown was simulated over 3 hrs. In the first hour, the simulated power cycled down to 0.1% of cycle 10B's EOC average LHGR to approximate decay heat. In the second hour, the simulated coolant inlet temperature was reduced to the experimental PIE temperature of 305 K [10]. During the third hour, all the parameters were held constant to allow the simulation to reach equilibrium before PIE measurements were made.

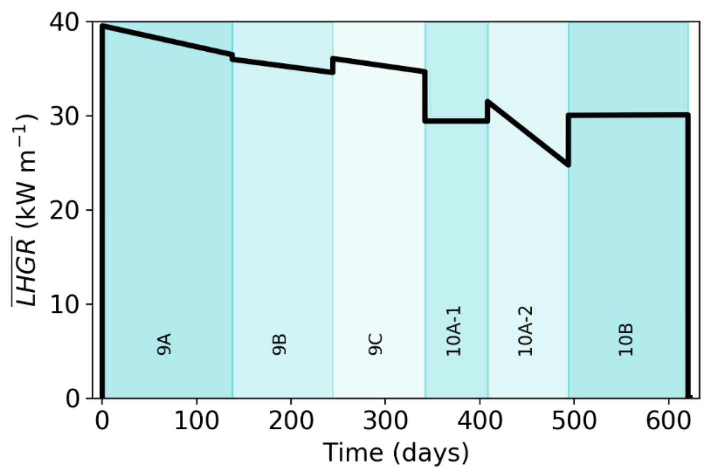

Figure 2. The average LHGR of the IFR-1 benchmark case throughout the six operating cycles.

During the fuel lifetime, the blanket slugs breed fissile isotopes and then begin to fission. However, it is unclear whether this was accounted for while calculating the average LHGR in the IFR-1 report [10]. For simplicity, this work assumed it was not. The axial peaking factor in the fuel slug was determined by fitting a fourth order polynomial to the axial power curve calculated in the report [10]. The polynomial was integrated over the active fuel column length to calculate the average simulated LHGR at that time. Then, the polynomial coefficients were divided by the average LHGR to determine the peaking factor polynomial. Isotopic gamma scans of ^{106}Rh from the report were used to approximate the average power of the blankets. The axial peaking factor was then defined by using the piecewise equation:

$$p(z) = \begin{cases} (m_b z + b_b) bu^*, & 0 \le z < z_b \\ a_0 + a_1 z_f + a_2 z_f^2 + a_3 z_f^3 + a_4 z_f^4, & z_b \le z \le z_t, \\ (m_t z + b_t) bu^*, & z_t < z \le 1.244 \end{cases}$$
$$z_f = z - z_b,$$
$$bu^* = \frac{bu}{bu_{ref}}, \tag{9}$$

where bu is the peak burnup; bu_{ref} is a reference burnup; bu^* is the normalized burnup; z is axial position; z_b and z_t are the bottom and top positions of the active fuel column, respectively; z_f is the axial position relative to the fuel column; and the remaining values are fitting coefficients. The fitting coefficients and reference burnup are given in

Table *1*. Equation (9) is compared with the report's axial power curve in Figure 3.

Table 1. Constants and fitting parameters for Eq. (9).

Constant	Value
a_0	0.68687
a_1	2.6352
a_2	-3.20026
a_3	1.35×10^{-5}
a_4	2.69×10^{-5}
b_b	0.084
b_t	0.416
bu_{ref}	5 at. %
m_b	0.279 m^{-1}
m_t	-0.301 m^{-1}
z_b	0.165 m
z_t	1.079 m

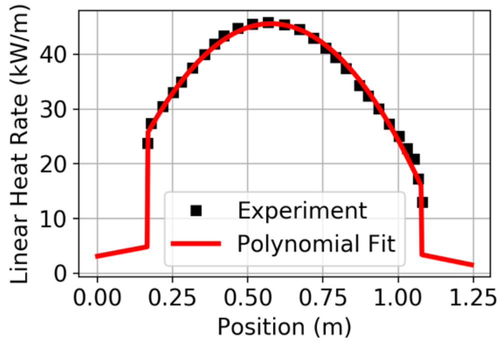

Figure 3. Comparison of the legacy and simulated LHGR profiles at an average LHGR of 37.1 kW m^{-1} and a peak burnup of 5%.

There are three points to consider regarding Eq. (9). First, there was a discrepancy between the axial power profile from the 2011 report used to create Eq. (9) [10] and that reported in the 2012 IFR-1 paper [17]. According to an author of both documents, the 2011 report has the more accurate profile [18]. Second, in reality, the axial peaking factor changes with burnup. For this work, it is assumed to be constant because only one profile was calculated during the experiment [10, 17]. Third, Eq.(8) was satisfied only within the active fuel column due to the assumption that the legacy power profile did not include power generated in the blanket. At 10 at. % peak burnup, $LHGR(t,z)$ was 6% higher than $\overline{LHGR}(t)$ due to the blankets.

3.3. ADDITIONAL PARAMETERS

BISON supplied many of the U-10Zr, U-19Pu-10Zr, and D9 material properties internally [20]. However, users must provide others to specify fuel, cladding, and coolant properties. This section lists the material properties used in the IFR-1 benchmark case, except for those called from within BISON. The parameters are sorted by material and tabulated with units and references. Any parameters that required additional derivation or discussion are also explained.

Table 2 contains the material parameters for the U-19Pu-10Zr fuel slug. The parameters are for models that include heat transport, thermal expansion, solid mechanics, solid fission product swelling, gaseous fission product swelling, and fuel creep. The anisotropic swelling factor is a value entered as input to control the anisotropy of the predicted fuel swelling. A value of -1 corresponded to 100% axial swelling, a value of 0 was isotropic swelling, and a value of 1 was 100% radial swelling. Metallic fuels swell preferentially in the radial direction, so a value of 0.5 (75% radial swelling) was used [23].

Table 2. Material parameters of the U-19Pu-10Zr fuel slug.

Parameter	Value	Reference
Anisotropic swelling factor	0.5	[23]
Atom fraction of Pu	0.16	[24]
Atom fraction of Zr	0.226	[24]
Average energy per fission	3.159×10^{-11} J	[10]
Coefficient of thermal expansion	17.3×10^{-6} K^{-1}	[24]
Initial density	15,800 kg m^{-3}	[24]
Fast flux factor	8.64×10^{14} n J^{-1} m^{-1}	[10, 19]
Thermal expansion reference temperature	295 K	

The coefficient of thermal expansion (CTE) for U-19Pu-10Zr, as well as CTEs of other materials, had to be derived. The thermal expansion equation from Janney [24] is nonlinear, but the BISON model used in this work required a linear thermal expansion equation [20]:

$$\frac{\Delta L}{L_0} = \alpha(T - T_0), \tag{10}$$

where L_0 is the reference length at temperature T_0, T is the current temperature, α is the CTE, and ΔL is the displacement or change in length. A least-squares approximation was used to linearize the thermal expansion equation. The slope of the linear equation was used as the CTE, and the reference temperature was set to the initial temperature of 295 K for all materials to maintain as-manufactured dimensions.

The fast flux factor was the ratio of fast neutron flux (n m^{-2} s^{-1}) to LHGR (W m^{-1}). It was approximated by dividing the peak total fast neutron fluence (15.4×10^{26} n m^{-2} [10]) by the time integral of $\overline{LHGR}(t)$ over the experiment lifetime (1.78×10^{12} J m^{-1} [19]) to get 8.64×10^{14} n J^{-1} m^{-1}.

Table 3 provides the material parameters for the blanket slugs. The anisotropic swelling factor was the same as for the fuel slug. The density and atom fraction of Zr were different due to the blankets' different composition. The CTE was linearized using the same method as the fuel slug but by using a nonlinear thermal expansion equation for U-10Zr [24].

Table 3. Material parameters of the U-10Zr blankets.

Parameter	Value	Reference
Anisotropic swelling factor	0.5	[23]
Atom fraction of Zr	0.225	[24]
CTE	16.6×10^{-6} K^{-1}	[24]
Initial density	16,310 kg m^{-3}	[24]

BISON developers derived BISON's empirical fission gas swelling and FGR model to match experimental observations [20]. As such, it had multiple adjustable parameters. The values used in this work are given in Table 4 and were provided by a BISON developer [25] who calibrated the models to match EBR-II data from Pahl and Wisner [26].

Table 4. Input parameters of the fission gas swelling and FGR models.

Parameter	Value	Reference
Bubble number density	2.09×10^{19} m^{-3}	[25]
Critical porosity	0.17195	[25]
Initial FGR fraction	0.558	[25]
Interconnection initiating porosity	0.125	[25]
Interconnection terminating porosity	0.2185	[25]
Post-critical FGR fraction	0.777	[25]

Table 5 provides the material parameters for the D9 cladding. All were taken from Hofman et al. [22]. The CTE was determined in the same way as described for the fuel slug. The Poisson's ratio and Young's modulus were both calculated from the Hofman et al. correlations [22] at an assumed temperature of 733 K.

Table 5. Material parameters of the D9 cladding.

Parameter	Value	Reference
Initial density	7,761 kg m^{-3}	[22]
CTE	1.9×10^{-5} K^{-1}	[22]
Poisson's ratio	0.35	[22]
Young's modulus	1.645×10^{11} Pa	[22]

The material parameters for liquid Na used in the gap and coolant are given in Table 6. The coolant inlet mass flux was not measured during the experiment. Instead, the FFTF design coolant velocity (7.01 m s^{-1} [15]) was multiplied by the Na density at the coolant inlet temperature of 622 K (866.9 kg m^{-3} [27]). However, the velocity had considerable uncertainty because the design velocity was published in 1980 before FFTF began operation. It is unknown whether the velocity was adjusted after the reactor began experimental operation or for individual experiments.

Table 6. Material parameters of the sodium coolant and plenum

Parameter	Value	Reference
Coolant inlet mass flux	6,079 kg m^{-2} s^{-1}	[15, 27]
Coolant inlet pressure	1.02×10^{6} Pa	[15]
Plenum pressure	84,000 Pa	
Rod pitch[a]	8.23×10^{-3} m	[10]
Thermal conductivity	61 W m^{-1} K^{-1}	[27]

[a]Equal to the pin diameter plus spacing wire diameter

The initial plenum pressure was not included in the available IFR-1 reports [10, 16, 17]. As such, a sub-atmospheric pressure representative of the glove box fabrication method used for the IFR-1 pins was assumed. The thermal conductivity was input into BISON as a constant, but Fink and Leibowitz provided it as a function of temperature [27]. The constant value needed to be calculated at a correct sodium temperature, but the predicted temperature profile is partially determined by the thermal conductivity. A simplified mathematical expression of this is $k = f(T), T = g(k)$, where f and g are functions, k is the thermal conductivity, and T is the gap temperature. The thermal conductivity listed in Table 6 was chosen by iteration. A guess T was used to calculate k. Then that value of k was used in a simulation. The gap temperature at cycle 9A BOC was used as a new guess T, and the process was repeated. Subsequent development has added the capability to input thermal conductivity as a function of temperature, so future work can avoid iterations like these.

3.4. AVAILABLE DATA FOR COMPARISON

One goal of this work was to compare BISON simulation results with legacy measurements and calculations. To do so, it was necessary to determine which data were measured or calculated and which of those data BISON could replicate. Seven legacy measurements and calculations (hereafter referred to as legacy values) that could be directly compared to the BISON predictions were identified:

1. calculated peak burnup at the end of most cycles,
2. calculated peak cladding temperature at the beginning and end of each cycle,

3. measured coolant outlet temperature during cycle 9A—the only cycle for which the INL report [10] included these measurements,
4. measured cladding radial dilation at the time of PIE,
5. measured cladding axial elongation at the time of PIE,
6. measured fuel axial elongation at the time of PIE, and
7. calculated FGR at the time of PIE.

The simulation results presented in Sections 4–6 were compared with these legacy values. Other measurements were also taken, such as axial isotopic distributions, radial constituent redistribution, Na penetration, and pin bowing. However, at the time of this work, BISON could not simulate these effects*. There were also quantities that BISON could calculate that were not measured during the experiment, such as stresses in the fuel and cladding and the full fuel temperature profile.

3.5. SIMULATION PROPERTIES

The 2D-RZ simulation mesh was built with BISON's internal mesh generation system. It consisted of four blocks: the cladding, the fuel column, and two blanket slugs. The fuel column and blanket slugs were attached as shown in Figure 1, but the cladding block did not initially contact the three slugs. The cladding wall included 4 radial elements and 400 axial elements. The fuel slug contained 6 radial and 300 axial elements, and each blanket contained 6 radial and 40 axial elements. A mesh refinement study was performed, and it was concluded that refining the mesh further would not alter the results.

Three primary variables were being solved by a system of nonlinear partial differential equations (PDEs): temperature, radial displacement, and axial displacement. Any other variables, such as burnup and FGR, were calculated based on the PDE variables' values. The initial conditions for the PDE variables were a uniform temperature of 295 K and zero displacements.

Boundary conditions for the axial displacement were zero-value Dirichlet conditions at the bottom of the cladding and bottom of the lower blanket slug. The only boundary condition for radial displacement was a zero-value Dirichlet condition at the center line of the fuel and cladding, which was the line of symmetry. Boundary conditions for the temperature included a zero-flux Neuman condition at the center line, more complex functions controlling heat transfer across the gap between the fuel and the cladding, and a coolant flow model that governed heat transport from the cladding to the coolant [20]. The coolant flow model also included feedback that allowed the coolant to increase in temperature and expand as it moved up the fuel pin.

As the meshes displaced, BISON used a finite element method (FEM) contact model [20]. However, the treatment of friction as two blocks move against one another can be somewhat complicated in solid mechanics solvers. There were three available options for modeling friction in BISON [20]. The simplest was to not include friction and allow blocks to freely slide against one another. The second option was to use a glued contact model (i.e., mesh points on fuel and cladding surfaces remain connected after achieving contact due to swelling). The third option, which was also the most computationally complex, was to actually model friction forces between the blocks. This required an additional friction coefficient parameter. The primary (i.e., baseline) simulation used the frictionless contact model because it was the most computationally inexpensive. However, the other contact models were also simulated. Their effects are discussed in Section 5.

4. BASELINE SIMULATION

* Constituent redistribution and Na infiltration models were under active development at the time of this work.

4.1. SETUP

The baseline simulation used all of the parameters listed in Section 3 and the frictionless contact model. It represented the best approximation of the IFR-1 experiment based on the available data. The simulation input file was added to the BISON repository and could be updated in the future as models are improved or if more relevant data are found.

4.2. RESULTS

Figure 4 shows the FEM mesh at several times during the simulation. The mesh in the figure was compressed by a factor of 20 in the axial direction to facilitate viewing. All three primary variables are shown in the figure. The temperature is represented by the mesh color, and displacements appear as changes to the mesh dimensions. The blankets are not explicitly labeled but can be distinguished as the regions with lower temperatures and displacements above and below the active fuel column. The representations in black for 0 days and 622 days represent simulated dimensions that correspond to the time of as-fabricated measurement and PIE, respectively.

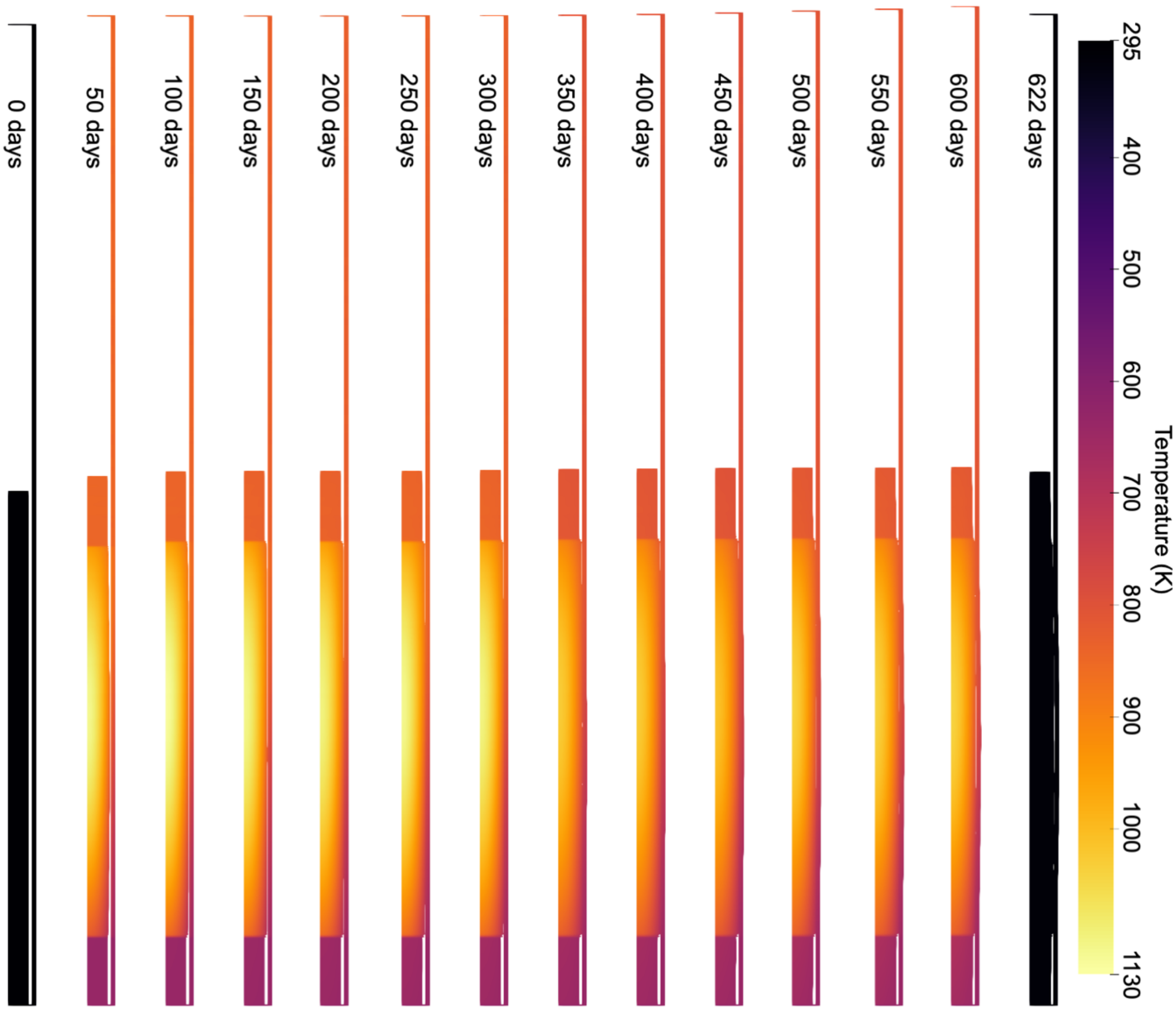

Figure 4. Predicted temperature and displacement results from the baseline BISON simulation. The mesh was compressed by a factor of 20 in the axial direction to make it easier to view. Simulation times are given near the top of each image. Color indicates temperature. Displacements are shown through dimensional changes of the mesh.

Comparisons are made between the predicted results and legacy values in Figure 5. In all seven plots, predicted results are in red and legacy values are in black. Plot 5(a) shows predicted and legacy peak burnups throughout the experiment. The simulation agreed very well with the experiment. Plot 5(b) shows the peak cladding temperatures throughout the experiment. The predicted results were biased (i.e., had a consistent error) by about 43 K; this difference is discussed later in the paper. Plot 5(c) shows the predicted coolant outlet temperature through the entire experiment and the measured legacy coolant outlet temperature during cycle 9A. Once again, the BISON simulation was biased, this time by an average of 23 K.

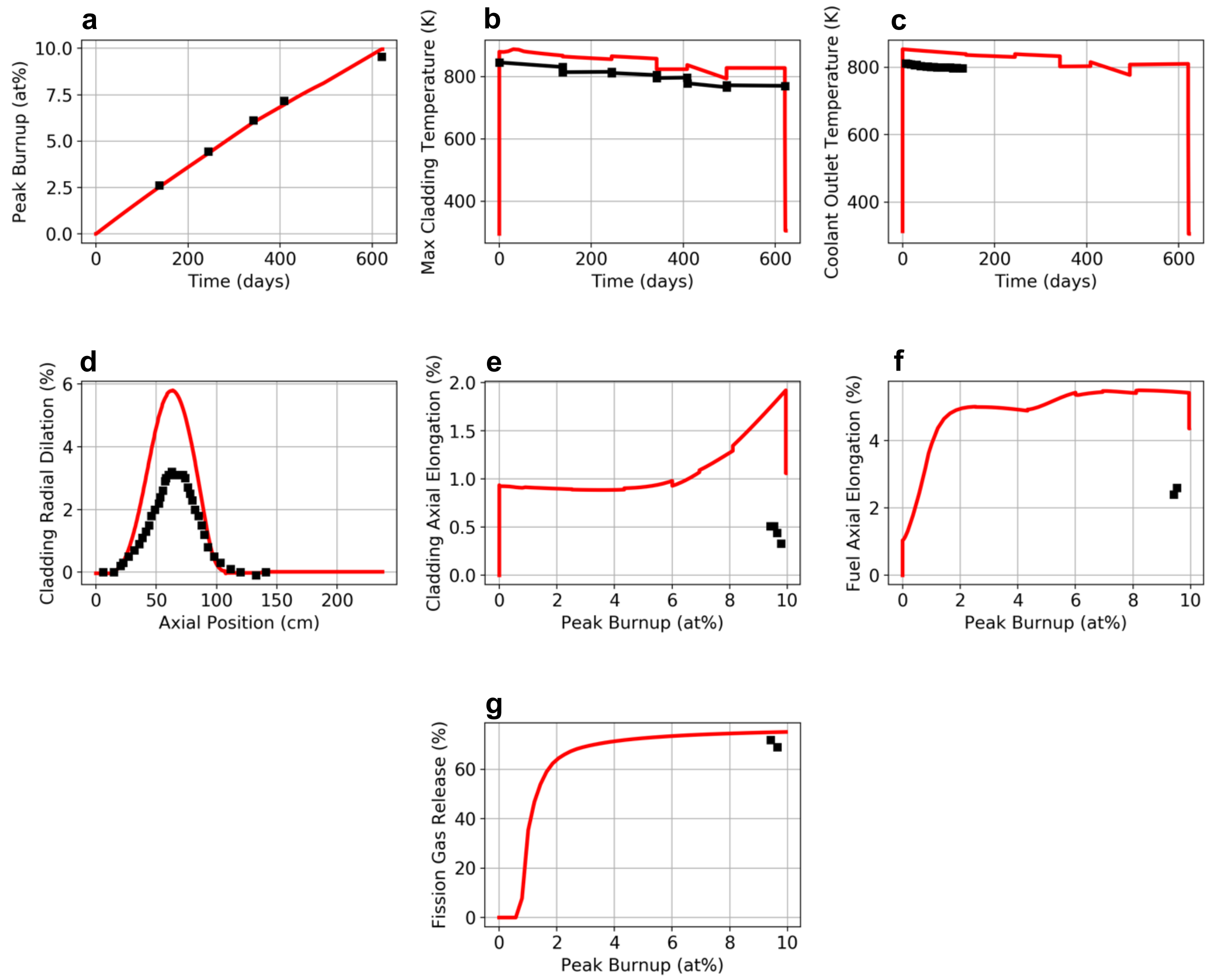

Figure 5. Comparison of BISON baseline predictions (red) and legacy values (black). All available data from U-19Pu-10Zr pins are included. The subplots show a) peak burnup, b) maximum cladding temperature, c) coolant outlet temperature, d) cladding radial dilation at PIE conditions, e) cladding axial elongation, f) fuel axial elongation, g) FGR fraction.

Plot 5(d) shows the predicted and legacy PIE cladding radial dilation. The measured peak cladding dilation was about 3.2%, and the simulation predicted 5.8% dilation. Plot 5(e) shows the cladding axial elongation. Thermal expansion and contraction during temperature changes can be seen as near-vertical lines at the beginning and end of the simulation. Predicted results are shown throughout the irradiation lifetime but were only measured experimentally during PIE at end of life (EOL). The four legacy values fell within the range of 0.33 to 0.51% elongation, and the simulated cladding axial elongation was 1.06% at EOL PIE conditions. Plot 5(f) shows the predicted and legacy fuel axial elongation. Once again, the predicted results are shown throughout the irradiation, and the legacy measurements were taken only at PIE. The fuel slug elongated 2.5%, and the simulation predicted 4.4% elongation. Plot 5(g) shows the FGR behavior for which the simulation compared well with PIE results. The legacy values were 69 and 72%, and the simulated FGR was 75%.

BISON-predicted peak stress components are shown in Figure 6 for reference. The subplots show radial, axial, and hoop stresses in the fuel, cladding, and blankets. The maximum values (tensile stress) are shown in red while the minimum values (compressive stress) are shown in blue. However, since no legacy values could be found for the stresses in the IFR-1 experiment, the accuracies of these predictions are unknown.

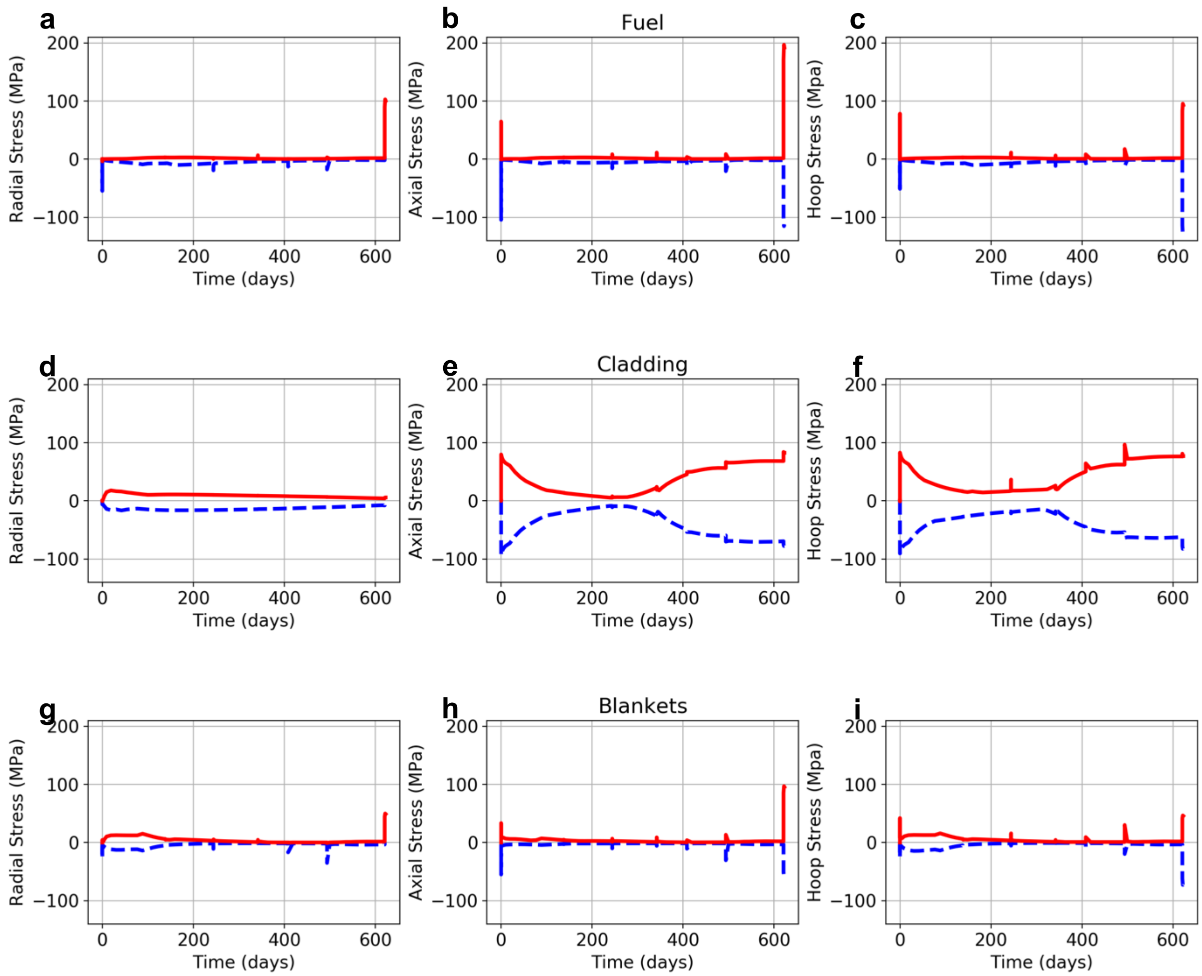

Figure 6. BISON baseline predictions of the minimum and maximum radial, axial, and hoop stresses in the fuel, cladding, and blankets. The maximum (tensile) stresses are shown with solid red lines, and the minimum (compressive) stresses are shown with blue dashed lines. The subplots show a) fuel radial stress, b) fuel axial stress, c) fuel hoop stress, d) cladding radial stress, e) cladding axial stress, f) cladding hoop stress, g) blanket radial stress, h) blanket axial stress, i) blanket hoop stress.

4.3. DISCUSSION

The predicted burnup and FGR results compared well with the legacy values. The agreement in burnup results indicates that the power history constructed for this benchmark case was reasonably accurate. Burnup is a calculated value based on the fuel composition and the total power produced by the pin. The legacy and simulated values likely used similar calculations, so to get the same results, they must have had similar compositions and power histories. The agreement in FGR results suggests that the FGR behavior of FFTF pins was similar to the FGR behavior of EBR-II pins of the same composition and that EBR-II data might be able to be used to fit functions that are accurate for FFTF pin. However, that cannot be determined conclusively because the data here represent only a single experiment at a single burnup.

Additional comparisons with more data would provide evidence that the burnup model was interchangeable between reactors.

The cladding and coolant outlet temperatures of the simulation were biased. The cladding temperature was not directly measured during the experiment. According to the IFR-1 report [10], the peak cladding temperature was approximated by adding 40 K to the measured coolant outlet temperature. However, the temperatures listed in the IFR-1 report actually vary by about 32 K. The reason for this discrepancy was unclear. Given the uncertainties in the legacy cladding temperature and the coolant inlet mass flux parameter, these results might be reasonable. The potential impact of these inconsistencies is examined in Section 6.4 by applying sensitivity analysis to investigate the effects of coolant mass flux on the predicted temperatures.

The three measured dimensional changes all saw significant differences between the BISON simulation and the legacy measurements. BISON consistently predicted more dilation and elongation than the experiment measured, indicating that BISON over-predicted axial and radial swelling. However, these measurements were results of the integrated effects of many phenomena and properties. Swelling, creep, FGR, friction, fuel-cladding chemical interactions (FCCI), and solid mechanics all influenced these values. Determining the specific source of the discrepancies would require considerable effort.

The BISON simulation was adjusted to test the effects of friction and FCCI. The results are presented in Section 5. Then, a sensitivity study was used to determine the effects of individual models. Those results are presented in Section 6.

5. FUEL AND CLADDING INTERACTION SIMULATIONS

The simulation in Section 4 used a frictionless contact model because it is the most computationally efficient. However, there are two other BISON contact models that can be used to account for the blocks' movements against one another: glued contact and frictional contact. The glued contact model behaved similar to one of the effects of FCCI, fuel and cladding bonding, which can cause the fuel to permanently bond to the cladding. Note that while the BISON glued contact model is a mechanical model, fuel and cladding bonding is a chemical effect, not a mechanical one, so the model can only be used as a rough approximation. The frictional model used a friction coefficient to add resistance to shear motion between the fuel and cladding. The baseline simulation was adjusted for simulations by using each of these models. The predicted results are given in this section.

5.1. SETUP

Switching between the frictionless and glued models in BISON is a simple process that only required changing one line of the input file. However, implementing the friction model was more complex. BISON used an Augmented Lagrangian model for frictional contact [20], which required more iterations to solve. It also requires the addition of a unitless friction coefficient. For UO_2, a friction coefficient of 0.3 or 0.4 was typically applied [20]. For metallic fuels, the value was unknown, so four values were used for parametric evaluation: 0.5, 1.0, 1.5, and 2.0.

5.2. RESULTS

The comparisons of the dimensional changes that used glued contact against legacy data are shown in Figure 7. The burnup, temperatures, and FGR were identical to the baseline case and are not shown in the figure. Once again, predicted results are in red and legacy data are in black. Plot 6(a) compares the cladding radial dilation. The glued simulation predicted 2.7% dilation, slightly lower than the actual dilation of 3.2%. Glued contact improved the BISON prediction. Plot 6(b) compares the cladding axial elongation. This is only marginally different from the baseline case with a final predicted elongation of 1.02%. Plot 6(c) compares the fuel axial elongation. In this case, the predicted results worsened. BISON predicted that the fuel would elongate 6.2%—significantly more than the legacy 2.5% and the baseline 4.4%.

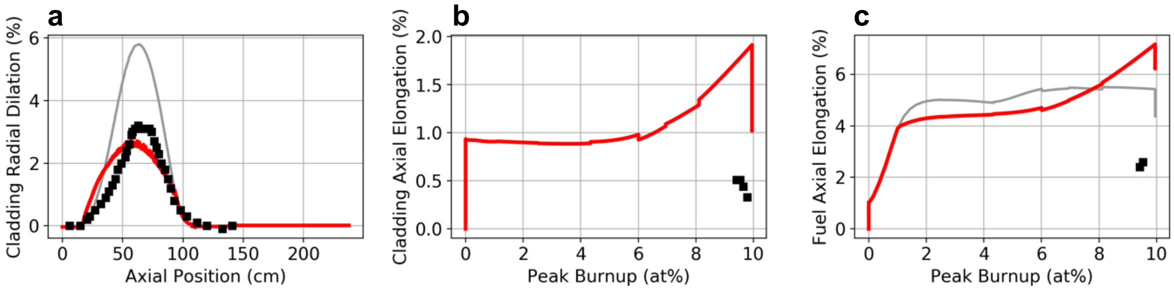

Figure 7. Comparison of the dimensional changes predicted by BISON that use glued contact (red), the baseline predictions (gray), and the legacy results (black). Subplot a) shows the cladding radial dilation. Subplot b) shows the cladding axial elongation. Subplot c) shows the fuel axial elongation.

The predicted results from the friction simulations with all four friction coefficient values were identical to the frictionless baseline simulation. Their predictions are not shown here.

5.3. DISCUSSION

Initially, glued contact reduced the fuel elongation. At 1.1% peak burnup and 4% elongation (corresponding to the time of fuel-cladding contact in the simulation), Plot 6(c) shows that the elongation in the glued case plateaued at a noticeably lower value compared to the baseline case. By 4% peak burnup, it only reached 4.4% elongation, but at the same burnup, the baseline case had reached 4.9% elongation. However, after 6% burnup fuel elongation of the glued case began accelerated. This correlates to the onset of cladding axial elongation, as shown in both plots 5(e) and 7(b).

The similar increase rates between cladding and fuel elongation at the same burnups suggests that the cladding void swelling-induced elongation caused additional fuel elongation. This is possible because the cladding is much stiffer than the fuel and the two are “glued” together in the simulation space. The more elongated fuel put less radial mechanical stress on the cladding, compared to the baseline case, which would explain the smaller cladding dilation results shown in plot 7(a).

In previously reported IFR-1 BISON simulations [19], the baseline case under-predicted cladding dilation, predicted no cladding elongation, and over-predicted fuel elongation. In that work, adding friction improved the predicted dimensional changes. In this work, the baseline case over-predicted all three measurements, although the fuel elongation was more accurate than in the previous work. An examination of the BISON source code found that the D9 swelling and creep models had been recently updated and now predict more dilation and elongation. This appears to have resulted in a simulated contact pressure that was insufficient for friction to govern the simulated dilation and elongation behaviors. Therefore, the baseline case was the most physically accurate and computationally efficient contact model at this time.

6. SENSITIVITY STUDIES AND SIMULATION TUNING

Since the use of alternative contact models (i.e., friction and glued contact) did not improve BISON's predictions on cladding and fuel elongations compared to legacy results, a study was performed to examine several of the physics models. A main effects study based on orthogonal array sampling [28, 29] was performed to identify the models to which the dimensional changes were most sensitive.

Once models that could be contributing to the errors were identified, the question turned to whether the errors could be contributed to poor calibration of the models and/or errors in legacy measurements, or if the models themselves were inaccurate. As a preliminary investigation, the benchmark was tuned in two cases. In the first case, parameters chosen based on the main effects study were used to try to improve the dimensional changes. If the benchmark can be successfully tuned, then a more comprehensive study can be used to improve BISON metallic fuel predictions. If, however, the benchmark cannot be tuned, it is evidence that the models are not accurately reflecting the physics. In the second case, the coolant mass flux was tuned to improve the predicted temperature profile. If that can be successfully tuned, it may suggest that the model calibration and/or uncertainty in the BISON inputs were the cause of the error.

It is not recommended to use the tuned parameter values in other BISON simulations because there was no physical basis for changing the values nor is there evidence that the tuned values would improve the predicted results of other simulations.

6.1. MAIN EFFECT STUDY SETUP

Four models that affected fuel and cladding dilation and elongation were chosen for variation: fuel swelling, FGR, cladding swelling, and cladding creep. In the case of fuel swelling, cladding swelling, and cladding creep, multipliers were applied to the models' values to reduce or enhance their effects. For the sake of consistency, every multiplier used the same three values: 0.9, 1.0, and 1.1. The FGR model had six parameters (Table 4). The post-critical FGR fraction was varied because it controlled the FGR model at high burnup, which was the only condition with legacy data to compare against. It was varied by ±10% of its original value to approximate the same relative variations as the multipliers. The fuel anisotropy factor was also varied to have values of 0.35, 0.5, and 0.65. These corresponded to 75% ± 7.5% of the swelling that occurs in the radial direction.

This resulted in five varied parameters with three values each. One simulation ran by using each unique combination of values, resulting in $3^5 = 243$ simulations. The seven response functions were then measured for each simulation. For each unique input parameter value, the predictions for the 81 simulations that used that unique value were averaged so that the change from that individual parameter could be measured across its three values.

6.2. MAIN EFFECT STUDY RESULTS

Figure 8 shows the complete main effect study results. The individual predictions are shown in gray, and the averages are shown in red. None of the model parameters had any effect on the burnup or coolant outlet temperature predictions, so those results are not included. Figure 8(a) shows the predictions for the highest cladding temperature reached over the entire simulation. The fuel swelling multiplier had the largest effect, but the anisotropy factor also had an effect.

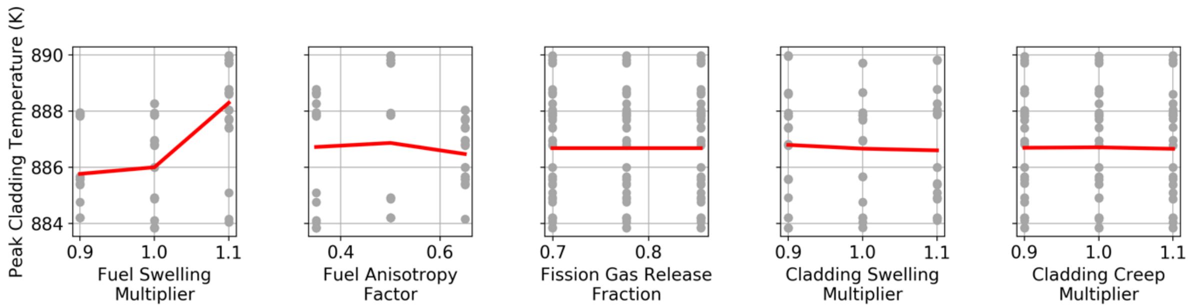

Figure 8(a). Model effects on peak cladding temperature. The range of temperatures only varied by 6 K, but the parameter with the largest effect was the fuel swelling multiplier.

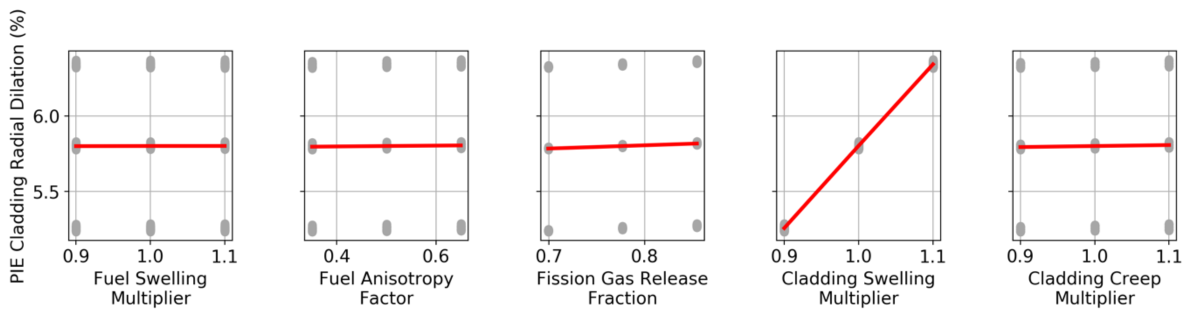

Figure 8(b). Model effects on cladding dilation. The cladding swelling multiplier was the only parameter to have an effect.

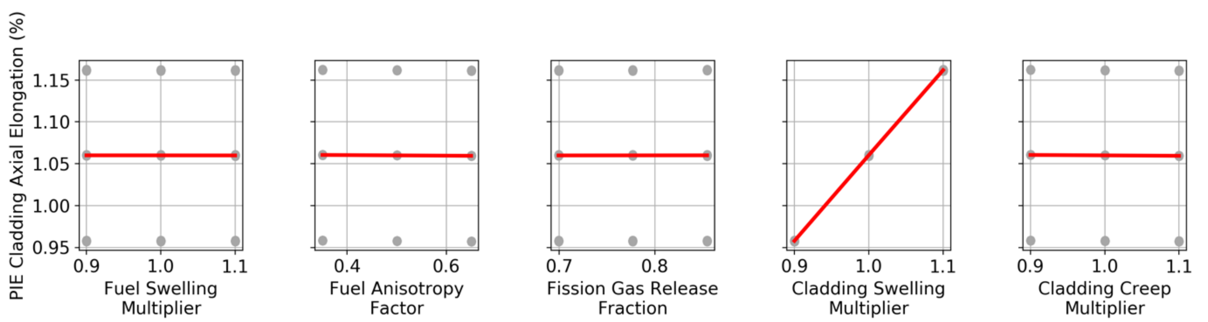

Figure 8(c). Model effects on cladding elongation. The cladding swelling multiplier was the only parameter to have an effect.

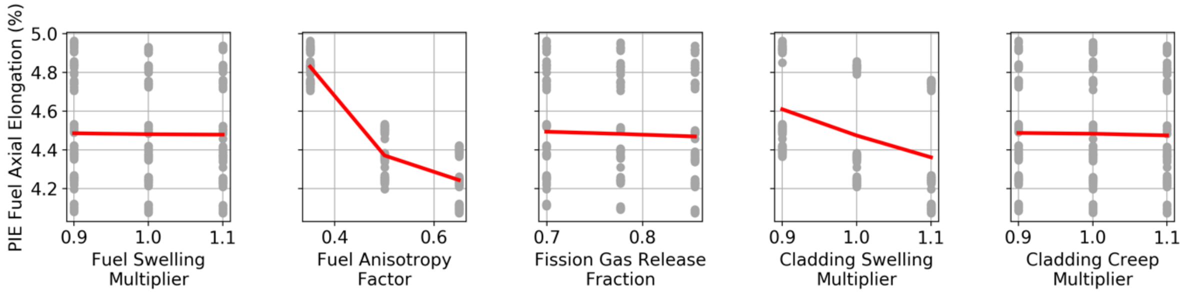

Figure 8(d). Model effects on fuel elongation. Several parameters affected it, but the fuel anisotropy factor had the largest effect.

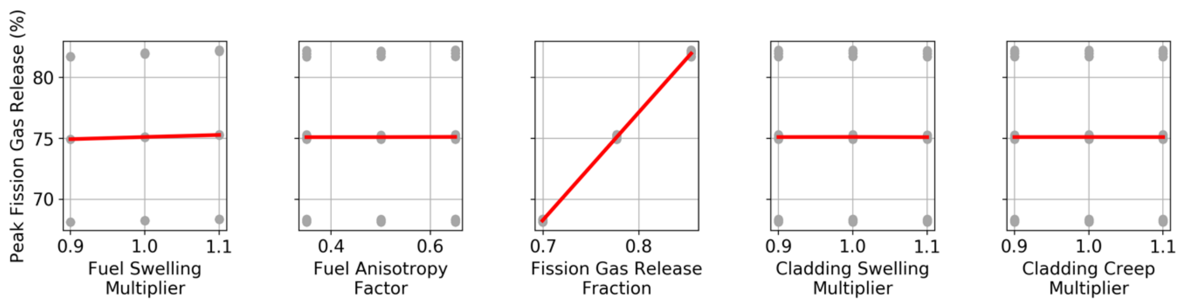

Figure 8(e). Model effects on FGR. The FGR fraction was the only parameter to have any effect.

Figure 8(b) shows the predictions of the study on cladding radial dilation at PIE. The cladding swelling multiplier was the only parameter to affect it. This indicates that for this set of conditions, BISON does not simulate appreciable fuel cladding mechanical interactions (FCMI) or stress induced in the cladding by fuel swelling. Figure 8(c) shows the predictions of cladding axial elongation. Once again, the cladding swelling multiplier was the only parameter to have an effect. Figure 8(d) shows the parameter effects on fuel axial elongation. The cladding swelling multiplier and fuel anisotropy factors had effects, although the cladding axial swelling effect on fuel elongation is not clearly supported by experimental observation, as discussed in Section 5.3. Finally, Figure 8(e) shows the effects on FGR. Only the FGR fraction had any effect.

The cladding swelling multiplier affected all three calculated dimensional changes and none of the other predictions, making it an excellent candidate for tuning the simulation. However, it alone could not tune all three calculated dimensional changes because it had a positive correlation to cladding dilation and elongation but a negative correlation to fuel elongation. Decreasing the cladding swelling multiplier would decrease cladding dilation and elongation but increase fuel elongation. Therefore, the fuel anisotropy factor was also tuned.

6.3. DIMENSIONAL PARAMETER TUNING SETUP

Two parameters were tuned to improve three result values: peak cladding dilation at EOL PIE, peak cladding elongation at EOL PIE, and peak fuel elongation at EOL PIE. Let $\vec{\epsilon}$ represent the 3×1 vector of differences between these three values and the averages of the available legacy values, $\vec{x}$ represent the 2×1 vector of input values (cladding swelling multiplier and fuel anisotropy factor), and $\vec{y}$ represent the input values with a constant:

$$\vec{y} = \begin{bmatrix} \vec{x} \\ 1 \end{bmatrix}. \tag{11}$$

Then assume a linear relationship:

$$\vec{\epsilon} = A\vec{y}, \tag{12}$$

where A is the 3 × 3 coefficient matrix. The coefficient matrix can be found by using three linearly independent input vectors $Y = [\vec{y_1}, \vec{y_2}, \vec{y_3}]$ and their corresponding error vectors $E = [\vec{\epsilon_1}, \vec{\epsilon_2}, \vec{\epsilon_3}]$, so that:

$$E = AY \iff A = EY^{-1}. \tag{13}$$

Now define a solution vector $\vec{\xi}$, so that:

$$\vec{0} \approx A \begin{bmatrix} \vec{\xi} \\ 1 \end{bmatrix}. \tag{14}$$

To solve for the solution vector, break A into two components, $A = [B \quad \vec{a}]$, where $\vec{a}$ is a 3 × 1 vector made from the third column of A, and B is a 3 × 2 matrix made from the first two columns. Rearrange to get:

$$\vec{0} \approx B\vec{\xi} + \vec{a} \iff -\vec{a} \approx B\vec{\xi}. \tag{15}$$

$\vec{\xi}$ can be found by using the least-squares method:

$$\vec{\xi} = -(B^T B)^{-1} B^T \vec{a}. \tag{16}$$

The simulation inputs were tuned by following this procedure, beginning with the baseline simulation and two guesses. The input and error vectors were updated with each simulation, resulting in a new tuned value. Depending on how the vectors were updated, the path could vary slightly but eventually reach the same values. However, the tuning process called for an anisotropy factor larger than what BISON allowed, so the maximum allowable value was used. The optimized cladding swelling multiplier and anisotropy factor were 0.5 and 1.0, respectively.

6.4. DIMENSIONAL PARAMETER TUNING RESULTS

The predicted results of the tuned simulation are shown in Figure 9. Burnup, temperatures, and FGR were unchanged compared with the baseline case, so only the dimensional changes are shown. Plot 8(a) shows the cladding dilation, which was nearly a perfect match to the entire legacy profile—not just the peak legacy value to which it was tuned. It reached a peak dilation of 3.0%. Plot 8(b) shows the cladding elongation. It decreased significantly to 0.54%. Plot 8(c) shows the fuel elongation. This result worsened compared with the baseline simulation. The fuel grew 5.5%, which was considerably higher than the measured elongation.

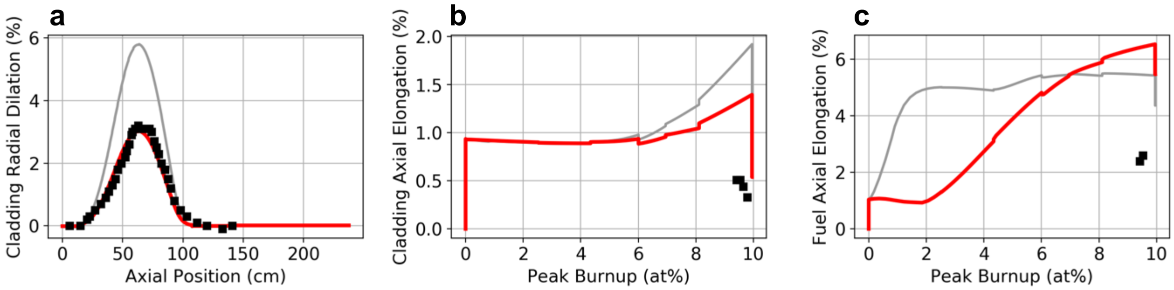

Figure 9. Dimensional changes comparison of dimensional-tuned BISON simulation (red), baseline BISON simulation (gray), and legacy values (black). Subplot a) shows the cladding radial dilation, subplot b) shows the cladding axial elongation, and subplot c) shows the fuel axial elongation.

6.5. TEMPERATURE PARAMETER TUNING SETUP

In addition to tuning the dimensional change predictions, a separate simulation was used to tune the temperature profile predictions. Because only one parameter was changed to vary one result, the method was somewhat simpler than the aforementioned dimensional tuning. Let ΔT be the average difference between the legacy peak cladding temperature and the simulation predicted peak cladding temperature and let $\dot{m}$ be the coolant inlet mass flux. Then, assume a linear relationship:

$$\Delta T = c_0 \dot{m} + c_1, \tag{17}$$

where c_0 and c_1 are constants. The constants are found by solving the equation for two coolant inlet mass flux, temperature difference pairs. Then, set the new mass flux to $-c_1/c_0$.

The coolant inlet mass flux was chosen for tuning because of the aforementioned unreliability of the referenced value. It was adjusted over several iterations to reduce the average error between the legacy and simulated peak cladding temperature. The tuned mass flux was 7,960 kg m^{-2} s^{-1}, which was 31% higher than the baseline case.

6.6. TEMPERATURE PARAMETER TUNING RESULTS

Figure 10 shows the predicted results of the tuned temperature simulations with the increased coolant inlet mass flux. The baseline predictions and measured values are also shown. Plot 9(a) shows the burnup, which did not vary significantly from the baseline simulation. Plot 9(b) shows the peak cladding temperature, and plot 9(c) shows the coolant outlet temperature. The average temperature differences between the simulation and the experiment were 5 K for the cladding and 1 K for the coolant. Plot 9(d) shows the cladding radial dilations. The reduction in the predicted temperature reduced the dilation compared with the baseline. Likewise, plot 9(e) shows that the cladding axial elongation was somewhat improved compared with the baseline simulation. Plot 9(f) shows the fuel axial elongation. The fuel was slightly more elongated compared with the baseline prediction. The FGR fraction is shown in plot 9(g). Like plot 9(a), it did not deviate from the baseline prediction.

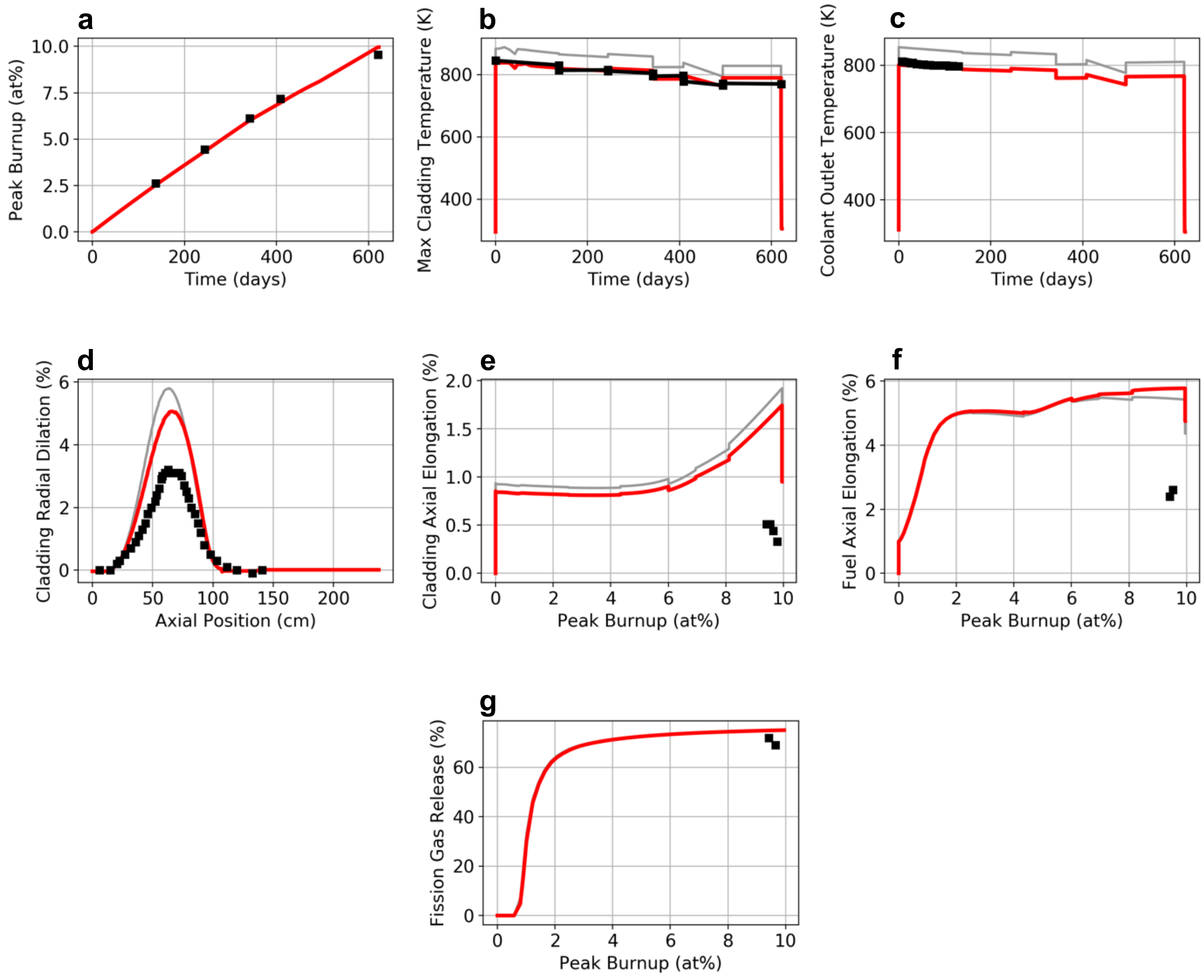

Figure 10. Comparison of temperature-tuned BISON simulation (red), baseline simulation (gray), and legacy values (black). Subplot a) shows the peak burnup was not affected. Subplots b) and c) show the maximum cladding temperature and coolant outlet temperature, respectively. Subplot d) shows the cladding radial dilation. Subplot e) shows the cladding axial elongation. Subplot f) shows the fuel axial elongation. Subplot g) shows the FGR fraction.

6.7. DISCUSSION

Possibly the most unexpected result of this sensitivity analysis and tuning studies was the effect of cladding dimensional changes on fuel dimensional changes. Figure 8(d) shows that the fuel swelling multiplier had only a negligible impact on the fuel axial elongation compared with the impact of the cladding swelling multiplier. This suggests that the cladding dimensions control the extents to which the fuel swells axially and radially. Once the fuel contacted the cladding, its radial dilation was constricted, so it began to swell axially. For this to be the case, the fuel must be too soft to deform the cladding. The tuned simulation predictions in Figure 9(a) show this very clearly. Despite 100% of the fuel swelling occurring in the radial direction, the fuel grew axially 5.5% because the reduced cladding dilation further constricted the fuel. This is also consistent with the glued contact simulation showed in Figure 7 in which cladding forced the fuel to stretch as it swelled. If this is the case, then the anisotropy factor cannot be measured experimentally after fuel-cladding contact occurs. It should only be measured by using low-burnup, pre-contact fuel.

The main effects study found that the fuel and cladding swelling models controlled the marginal fuel and cladding dilation and elongation behaviors more than creep and fission gas models. However, tuning the swelling models could not correct the simulation error. To correct the error in cladding and fuel dilation and elongation, it might be necessary to develop a more mechanistic model.

The predicted results of tuning according to temperature show that the over-predicted simulation temperature can be completely explained as a result of uncertainty in the model input parameters. This does not prove that inaccurate input parameters were the cause of the temperature discrepancy. To do that, a more certain value of the coolant inlet velocity must be found or determined. However, it was enough to conclude that the temperature profiles were reasonably accurate.

Additionally, correcting for the temperature improved the cladding dilation and elongation predictions. However, like the mechanical tuning simulation, improving the cladding prediction worsened the predicted fuel axial growth.

7. CONCLUSIONS

A benchmark case was designed and configured to simulate the IFR-1 experiment in the FFTF reactor. The benchmark was simulated by using BISON and was compared with IFR-1 legacy values and calculations. The burnup and FGR predictions compared well against legacy results. The simulated temperatures were somewhat higher than the previously measured and calculated experiment temperatures, but they were as accurate as could be expected given the uncertainty of the coolant inlet velocity (and hence mass flux), the LHGR, and other input parameters. BISON over-predicted the dimensional changes of the fuel and cladding. A sensitivity study was performed to determine which physical models could have been responsible for this, and the dimensional changes were found to be the most sensitive to the cladding swelling model and fuel swelling anisotropy. However, improvements in these two models alone would not correct the predictions, as indicated by an attempt to tune the simulation by using these parameters that resulted in increased axial elongation in the fuel.

The fuel swelling was limited by mechanical contact with the cladding. After fuel contacted the cladding, swelling was forced to occur in the axial direction irrespective of the degree of swelling anisotropy in the fuel. Therefore, any future attempts to measure the fuel swelling anisotropy should use low burnup fuel that has not come into contact with the cladding.

Future simulation and benchmarking work should incorporate additional irradiation experiments to compare simulations predictions with an expanded range of operating conditions, cladding and fuel materials, and measurements. These should especially focus on more complete dimensional change data to help pinpoint the behaviors that are causing the benchmark cases to have inaccurate swelling predictions. Future development on fuel and cladding interaction models, especially cladding swelling and FCCI, would be beneficial. As models are developed or improved, their effects can be measured by running this benchmark case again with the updated models. Future experiments should focus on low-burnup swelling anisotropy, friction, and bonding between the fuel and cladding, and they should always record the experimental coolant inlet flow rate.

ACKNOWLEDGMENTS

This work was funded by the DOE Office of Nuclear Energy (NE) Versatile Test Reactor (VTR) Project. The reported work resulted from studies that support a VTR conceptual design, cost, and schedule estimates for DOE-NE to make a decision of procurement. As such, it is preliminary.

The authors thank Stephen Novascone, Al Casagranda, and Adam Zabriskie of the INL BISON development team and Alexander Lindsay of the INL MOOSE development team for their valuable input in BISON fuel performance models in metallic fuels. The authors also thank Doug Porter for sharing his knowledge and experience with metallic fuels in general and the IFR-1 experiment in particular.

DATA AVAILABILITY

Simulation results can be made available upon request. BISON is export controlled with access granted on an individual basis. To apply for BISON access, visit https://bison.inl.gov. The input file for the baseline version of the IFR-1 benchmark case is distributed with the BISON code as a metallic fuel assessment case.

AUTHOR IMPACT STATEMENT

Ian Greenquist led the development of the IFR-1 benchmark case and wrote the manuscript text. Kaylee Cunningham developed the initial version of the IFR-1 benchmark case. Jianwei Hu helped with BISON model development and parameter selection. Jeffrey Powers led the benchmark development work at Oak Ridge National Laboratory (ORNL) and provided important technical feedback and manuscript editing. Doug Crawford led the fuel design team engaged with this work and provided technical editing.

DISCLAIMERS

The authors have no competing interests. Portions of this research have been previously published in an ORNL technical memo [19].

BIBLIOGRAPHY

[1] H. S. Aybar and P. Ortega, "A review of nuclear fuel performance codes," *Progress in Nuclear Energy,* pp. 127-141, 2005.

[2] D. Olander, "Nuclear fuels - Present and future," *Journal of Nuclear Materials,* vol. 389, no. 1, pp. 1-22, 2009.

[3] Y. I. Chang, "Technical Rationale for metal fuel in fast reactors," *Nuclear Engineering and Technoogy,* vol. 39, no. 3, pp. 161-170, 2007.

[4] T. Ogata and T. Yokoo, "Development and Validation of ALFUS: An Irradiation Behavior Analysis Code for Metallic Fast Reactor Fuels," *Nuclear Technology,* vol. 128, no. 1, pp. 113-123, 1999.

[5] S. L. Hayes, "SAFE: A computer code for the steady-state and transient thermal analysis of LMR fuel elements," Argonne National Laboratory ANL-IFR-221, Argonne, Illinois, 1993.

[6] US Department of Energy, "Secretary Perry Launches Versatile Test Reactor Project to Modernize Nuclear Research and Development Infrastructure," 28 February 2019. [Online]. Available: https://www.energy.gov/articles/secretary-perry-launches-versatile-test-reactor-project-modernize-nuclear-research-and. [Accessed 10 March 2020].

[7] US Department of Energy, "Versatile Test Reactor: World-Class R&D Enabled by Fast Neutrons," October 2019. [Online]. Available: https://www.energy.gov/sites/prod/files/2019/11/f68/19-50625_VTR_R7_0.pdf. [Accessed 10 March 2020].

[8] P. Hejzlar, R. Petroski, J. Cheatham, N. Touran, M. Cohen, B. Truong, R. Latta, M. Werner, T. Burke, J. Tandy, M. Garrett, B. Johnson, T. Ellis, J. Mcwhirter, A. Odedra, P. Schweiger, D. Adkisson and Gill, "Terrapower, LLC Traveling Wave Reactor Development Program Overview," *Nuclear Engineering and Technology,* vol. 45, no. 6, pp. 731-744, 2013.

[9] Third Way, "Keeping Up with the Advanced Nuclear Industry," 8 February 2018. [Online]. Available: https://www.thirdway.org/graphic/keeping-up-with-the-advanced-nuclear-industry. [Accessed 10 March 2020].

[10] D. L. Porter and H. Tsai, "Full-length Metallic Fast Reactor Fuel Pin Test in FFTF (IFR-1)," Idaho National Laboratory INL/EXT-12-25550, Idaho Falls, Idaho, 2011.

[11] Y. I. Chang, "The Integral Fast Reactor," *Nuclear Technology,* vol. 88, no. 2, pp. 129-138, 1989.

[12] E. L. Gluekler, "U.S. Advanced Liquid Metal Reactor (ALMR)," *Progress in Nuclear Energy,* vol. 31, no. 1/2, pp. 43-61, 1997.

[13] C. E. Till, Y. I. Chang and W. H. Hannum, "The integral fast reactor - an overview," *Progress in Nuclear Energy,* vol. 31, pp. 3-11, 1997.

[14] Hanford Site, "400 Area / Fast Flux Test Facility," [Online]. Available: https://www.hanford.gov/page.cfm/400areafftf. [Accessed 11 March 2020].

[15] C. P. Cabell, "A Summary Description of the Fast Flux Test Facility," Hanford Engineering Development Laboratory Report HEDL-400, Hanford, Washington, 1980.

[16] H. Tsai and L. A. Neimark, "Irradiation performance of full-length metallic IFR fuels.," Argonne National Laboratory Report ANL/CP-74935, Argonne, Illinois, 1992.

[17] D. L. Porter and H. Tsai, "Full-length U-xPu-10Zr (x=0, 8, 19wt.%) fast reactor fuel test in FFTF," *Journal of Nuclear Materials,* vol. 427, no. 1, pp. 46-57, 2012.

[18] D. Porter, Interviewee, [Interview]. 2019.

[19] I. Greenquist, K. M. Cunningham, J. Hu and J. J. Powers, "A Metallic Fuel Performance Benchmark Problem Based on the IFR-1 Experiment," Oak Ridge National Laboratory ORNL/TM-2020/1534, Oak Ridge, Tennessee, 2020.

[20] Idaho National Laboratory, "BISON Manual," Idaho National Laboratory, [Online]. Available: https://mooseframework.org/bison/. [Accessed 27 March 2020].

[21] J. D. Hales, R. L. Williamson, S. R. Novascone, G. Pastore, B. W. Spencer, D. S. Stafford, K. A. Gamble, D. M. Perez, R. J. Gardner, W. Liu, J. Galloway, C. Matthews, C. Unal and N. Carlson, "BISON Theory Manual-The Equations Behind Nuclear Fuel Analysis," Idaho National Laboratory INL/EXT-13-29930 Rev. 3, Idaho Falls, Idaho, 2016.

[22] G. L. Hofman, M. C. Bilone, J. F. Koenig, J. M. Kramer, J. D. B. Lambert, L. Leibowitz, Y. Orechwa, D. R. Pederson, D. L. Porter, H. Tsai and A. E. Wright, "Metallic Fuels Handbook," Argonne National Laboratory, Chicago, 1989.

[23] R. G. Pahl, D. L. Porter, C. E. Lahm and G. L. Hofman, "Experimental Studies of U-Pu-Zr Fast Reactor Fuel Pins in the Experimental Breeder Reactor-II," *Metallurgical Transactions A,* vol. 21, no. 7, pp. 1863-1870, 1990.

[24] D. E. Janney, "Metallic Fuels Handbook," Idaho National Laboratory INL/EXT-15-36520, Idaho Falls, Idaho, 2018.

[25] A. Casagranda, *BISON Metallic Fuel/VTR Training,* presented at Oak Ridge, Tennessee, Tennessee: Idaho National Laboratory, January 2020.

[26] R. G. Pahl and R. S. Wisner, "Steady-state Irradiation Testing of U-Pu-Zr Fuel to >18% Burnup," Argonne National Laboratory CONF-900804-25, Argonne, Illinois, 1990.

[27] J. K. Fink and L. Leibowitz, "Thermodynamic and transport properties of sodium liquid and vapor," Argonne National Laboratory ANL/RE-95/2, Chicago, 1995.

[28] G. Pastore, L. P. Swiler, J. D. Hales, S. R. Novascone, D. M. Perez, B. W. Spencer, L. Luzzi, P. Van Uffelen and R. L. Williamson, "Uncertainty and sensitivity analysis of fission gas behavior in engineering-scale fuel modeling," *Journal of Nuclear Materials,* vol. 456, pp. 398-408, 2015.

[29] D. C. Montgomery and G. C. Runger, Applied Statistics and Probability for Engineers, Hoboken, New Jersey: Wiley, 2011.